Phys Chem Minerals
DOI 10.1007/s00269-015-0744-y

ORIGINAL PAPER

Compressibilities of $MnFe_2O_4$ polymorphs

Lijin Ye[1] · Shuangmeng Zhai[2] · Xiang Wu[1] · Chaowen Xu[1] · Ke Yang[3] · Yuji Higo[4]

Received: 10 November 2014 / Accepted: 21 March 2015

Abstract The high-pressure behavior and stability of synthetic jacobsite $MnFe_2O_4$ have been investigated up to 39.55 GPa at room temperature by means of in situ synchrotron X-ray diffraction using diamond anvil cell and multi-anvil high-pressure apparatus. The $MnFe_2O_4$ spinel undergoes a phase transition at about 18 GPa to form a denser antiferromagnetic $CaMn_2O_4$-type (CM_{afm}) polymorph. The CM_{afm} $MnFe_2O_4$ is stable up to 39.55 GPa in this study and remains after decompression. Fitting the pressure–volume data using a third-order Birch–Murnaghan equation of state, the isothermal bulk modulus values and the first pressure derivatives were obtained as $K_0 = 169.7$ (35) GPa, $K_0' = 2.87$ (40) for spinel-type $MnFe_2O_4$ and $K_0 = 149.2$ (24) GPa, $K_0' = 3.98$ (19) for CM_{afm} $MnFe_2O_4$, respectively. If K_0' is fixed to 4, K_0 was obtained as 160.6 (11) GPa for spinel-type $MnFe_2O_4$ and 148.9 (7) GPa for CM_{afm} $MnFe_2O_4$. The effects of cation substitution on the isothermal bulk modulus and pressure for phase transition of Fe^{3+}-bearing spinels were discussed.

✉ Shuangmeng Zhai
zhaishuangmeng@vip.gyig.ac.cn

[1] Key Laboratory of Orogenic Belts and Crustal Evolution, MOE; School of Earth and Space Sciences, Peking University, Beijing 100871, China

[2] Key Laboratory of High-Temperature and High-Pressure Study of the Earth's Interior, Institute of Geochemistry, Chinese Academy of Sciences, Guiyang 550002, Guizhou, China

[3] Shanghai Synchrotron Radiation Facility, Shanghai Institute of Applied Physics, Chinese Academy of Sciences, Shanghai 201204, China

[4] Japan Synchrotron Radiation Research Institute, Sayo, Hyogo 679-5198, Japan

Keywords $MnFe_2O_4$ · High pressure · Equation of state · Synchrotron X-ray diffraction · Phase transition

Introduction

Spinel-structured minerals (spinels) are common accessory minerals in most kinds of crustal rocks. Spinels with the general chemical formula of AB_2O_4 can disorder over A and B sites, leading to a normal and an inverse structure. In the normal structure, divalent cations and trivalent cations are in tetrahedral site A and octahedral site B, respectively, while in the inverse structure, all divalent and half of the trivalent cations are in site B, with the rest of trivalent cations in site A (Levy et al. 2001). At ambient conditions, spinels have cubic structure (space group = $Fd\bar{3}m$, Z = 8).

The high-pressure phase transitions of spinels are of high relevance, because of the occurrence of their high-pressure polymorphs in nature (Chen et al. 2008) and their possible existence in the earth's mantle. Upon compression, phase transitions of cubic spinels to new denser polymorphs of $CaFe_2O_4$-type (space group *Pnam*) (e.g., $MgAl_2O_4$, Irifune et al. 1991; Ono et al. 2006), $CaMn_2O_4$-type (space group *Pbcm*) (e.g., Fe_3O_4, Fei et al. 1999), $CaTi_2O_4$-type (space group *Cmcm*) (e.g., $ZnTi_2O_4$, Wang et al. 2002) and ε-$MgAl_2O_4$-type (e.g., $MgAl_2O_4$, Liu 1978) have been reported. In the former three similar structures, Ca atoms are located in a dodecahedral site and Fe, Mn or Ti atoms in octahedral site. The octahedra share their corners and edges to form a compact network. The slight differences in modifications of the octahedra lead to two types of FeO_6 in $CaFe_2O_4$-type and a distorted MnO_6 in $CaMn_2O_4$-type, whereas a more symmetric CaO_8 in $CaTi_2O_4$-type (Yamanaka et al. 2008). These almost indistinguishable differences lead to several debates on the properties and

Published online: 03 April 2015

structure of post-spinel phases (Irifune et al. 2002). Additionally, a tetragonal distorted structure ($I4_1/amd$) could be adopted when $ZnGa_2O_4$ spinel was compressed to about 31 GPa (Errandonea et al. 2009) and $MgCr_2O_4$ spinel to about 20 GPa at room temperature (Yong et al. 2012). The tetragonal distorted structure of $ZnGa_2O_4$ changed to $CaMn_2O_4$-type polymorph at 55 GPa (Errandonea et al. 2009).

Fe^{3+}-bearing spinels are almost ubiquitous in lower crust and upper mantle, since the crystallization of magnetite (Fe^{3+}-rich spinel) will cause the cessation of the crystallization of chromite (Cr^{3+}-rich spinel) (Roeder 1994). These spinels have been considered to contribute to the crustal magnetism (Frost and Shive 1986; Levy et al. 2000) and are important indicators of oxygen fugacity in host rocks (e.g., magnetite, O'Neill and Wall 1987). A phase transition of $MgFe_2O_4$ from spinel to $CaMn_2O_4$-type structure has been reported at 25 GPa (Andrault and Bolfan-Casanova 2001). This transition also happens for $ZnFe_2O_4$ at 24 GPa to either $CaFe_2O_4$- or $CaTi_2O_4$-like structure (Levy et al. 2000) and for Fe_3O_4 at 23.6 GPa (Fei et al. 1999). Besides, Wang et al. (2003) reported that $CoFe_2O_4$ adopted the $CaFe_2O_4$-like structure at high pressure. Among these high-pressure experiments, a few spinels have been reported to decompose into oxide mixtures before post-spinel phase transition such as $MgAl_2O_4$ and $MgFe_2O_4$ (Ono et al. 2006; Levy et al. 2004). A comprehensive review on these transitions was published recently by Errandonea (2014).

In this study, we investigate the stability and compressibility of $MnFe_2O_4$ spinel up to pressure of 39.55 GPa at room temperature by means of in situ synchrotron X-ray diffraction using diamond anvil cell and multi-anvil high-pressure apparatus. This ferrite spinel has an inverse spinel structure whose fraction of tetrahedral sites occupied by Mn^{2+} has been found to be 0.81 ± 0.03 at 300 K (Hastings and Corliss 1956). A phase transformation is observed for this compound, and the structure of new phase was refined. The elastic parameters of $MnFe_2O_4$ polymorphs were obtained by fitting the obtained pressure–volume data. Combined with previous results, the effects of cation substitution on the isothermal bulk modulus and pressure for phase transition of Fe^{3+}-bearing spinels were discussed.

Experimental

The $MnFe_2O_4$ sample was prepared by a solid-state reaction. Reagent-grade MnO and Fe_2O_3 powders were mixed in the proportion corresponding to the $MnFe_2O_4$ stoichiometry, and the mixture was ground sufficiently and pressed into pellets with a diameter of 5 mm. The pellets were sintered at 1773 K for 24 h in argon atmosphere. A powder X-ray diffraction pattern confirms the sintered product is pure $MnFe_2O_4$ spinel. A mixture of $MnFe_2O_4$ plus 10 wt% Au, the internal pressure marker, was prepared for the high-pressure in situ X-ray experiments.

Two kinds of high-pressure experiments were performed. The high-pressure angle dispersive in situ X-ray diffraction (ADXRD) experiment was carried out at beamline BL15U1 of SSRF, China, using a diamond anvil cell (DAC) with a culet of 300 μm. The experimental techniques used in this study were similar to previous studies (Wu et al. 2013; Xu et al. 2014). A rhenium disk with an initial thickness of 260 μm was pre-intended to a thickness of 32 μm, where a hole with the diameter of 150 μm was drilled as the sample chamber. The sample was loaded within the pressure medium of silicone oil into the chamber. A monochromatic X-ray with a wavelength of 0.6199 Å was adopted, and the beam spot on the sample was about 5 μm in diameter. Two-dimensional images were collected for 10 s at different pressures and integrated by Fit2D software to obtain the one-dimensional diffraction patterns (Hammersley et al. 1996). Pressure was calculated using the equation of state of Au proposed by Tsuchiya (2003) from the volume determined using (111) and (200) diffraction lines since other diffraction lines are not available, which leads the uncertainties of the pressure within ±0.30 GPa, as shown in Table 1. XRD data were dealt with using Rietveld analysis by the GSAS-EXPGUI software (Larson and Von Dreele 2004) to obtain the lattice parameters.

On the other hand, the high-pressure energy dispersive in situ X-ray diffraction (EDXRD) experiment was conducted using a multi-anvil high-pressure apparatus, SPEED 1500, at beamline BL04B1 of SPring-8, Japan. The experimental method was similar to that described by Zhai et al. (2011, 2013). Kawai-type cell assembly composed of eight cubic second-stage tungsten carbide anvils with edge length of 26 mm and truncated edge length of 2 mm was adopted. A semi-sintered octahedron with 6.5 mm edge length made of MgO was used as the pressure medium, and pyrophyllite as the gasket. The tubing heater and sample capsule were made of TiB_2, for its high transparency for X-ray. A CCD camera and a Ge solid-state detector (SSD) were used to locate the sample and collect the X-ray diffraction patterns, respectively. During compression, the sample was heated to about 1000 K estimated from the temperature–power relationship of heater to release the deviatoric stress. The X-ray diffraction patterns were collected after quenching. The diffraction peak positions were determined using XrayAna program, and the lattice parameters were obtained by Refine program. Pressure was calculated using the equation of state of Au proposed by Tsuchiya (2003) from the volume determined using (111), (200), (220), (311) and (222) diffraction lines. Uncertainties in the pressure determination were mostly within ±0.10 GPa, as shown in Table 1.

Table 1 Lattice parameters of spinel-type and CM_{afm} $MnFe_2O_4$ at various pressures

P (GPa)	Spinel-type			CM_{afm}			
	a (Å)	V (Å^3)	P (GPa)	a (Å)	b (Å)	c (Å)	V (Å^3)
0.00 (7)	8.5157 (2)	617.54 (4)	0.00 (0)	9.8680 (1)	9.751 (1)	2.9435 (2)	566.46 (7)
0.83 (8)	8.4980 (4)	613.69 (9)	2.37 (6)	9.8293 (1)	9.704 (1)	2.9345 (2)	559.81 (6)
0.95 (5)	8.4979 (3)	613.67 (7)	3.74 (10)	9.7994 (1)	9.663 (1)	2.9234 (2)	553.64 (6)
1.75 (28)*	8.4830 (8)	610.51 (25)	5.39 (12)	9.7604 (1)	9.630 (1)	2.9125 (2)	547.51 (6)
2.66 (7)	8.4718 (4)	608.03 (7)	7.14 (8)	9.7258 (1)	9.594 (1)	2.9023 (2)	541.62 (6)
2.89 (7)	8.4650 (5)	606.57 (11)	9.20 (12)	9.6915 (1)	9.548 (1)	2.8916 (2)	535.15 (6)
3.45 (20)*	8.4591 (9)	605.31 (26)	9.71 (17)	9.6829 (1)	9.542 (1)	2.8896 (2)	533.96 (6)
4.37 (15)*	8.4442 (8)	602.06 (26)	10.37 (14)	9.6652 (1)	9.531 (1)	2.8839 (2)	531.32 (6)
4.44 (18)	8.4436 (5)	601.99 (11)	11.40 (17)	9.6597 (1)	9.522 (1)	2.8797 (2)	529.75 (6)
5.47 (22)*	8.4220 (9)	597.29 (26)	13.31 (11)	9.6306 (1)	9.488 (1)	2.8715 (2)	524.77 (6)
5.79 (18)	8.4194 (4)	596.83 (8)	13.64 (8)	9.6171 (1)	9.472 (1)	2.8682 (2)	522.55 (6)
6.12 (13)*	8.4161 (9)	596.10 (30)	15.06 (11)	9.6108 (1)	9.465 (1)	2.8660 (2)	521.42 (6)
7.31 (12)	8.4045 (5)	593.60 (10)	17.36 (12)	9.5793 (1)	9.423 (1)	2.8532 (2)	515.11 (6)
7.43 (21)*	8.3960 (8)	591.94 (24)	18.90 (17)	9.5575 (1)	9.404 (1)	2.8490 (2)	512.14 (6)
10.34 (19)	8.3592 (4)	583.90 (8)	19.87 (12)	9.5451 (1)	9.393 (1)	2.8451 (2)	510.17 (6)
10.44 (30)*	8.3611 (9)	583.25 (23)	21.74 (14)	9.5196 (1)	9.363 (1)	2.8379 (2)	505.90 (6)
12.56 (29)*	8.3232 (8)	576.55 (29)	23.34 (11)	9.4880 (1)	9.336 (1)	2.8304 (2)	501.42 (6)
13.19 (21)*	8.3131 (9)	574.56 (23)	24.63 (16)	9.4747 (1)	9.320 (1)	2.8258 (2)	499.05 (6)
13.49 (12)	8.3119 (4)	574.25 (8)	25.87 (19)*	9.4569 (1)	9.291 (1)	2.8170 (3)	495.00 (6)
16.87 (27)*	8.2721 (9)	565.98 (32)	26.79 (24)*	9.4389 (1)	9.279 (1)	2.8118 (3)	492.52 (6)
18.06 (9)	8.2536 (4)	562.25 (8)	28.82 (23)*	9.4234 (1)	9.249 (1)	2.8090 (3)	489.63 (5)
18.36 (23)*	8.2451 (9)	560.50 (22)	29.72 (21)*	9.4167 (1)	9.237 (1)	2.8056 (3)	488.02 (5)
			31.60 (14)*	9.3987 (1)	9.218 (1)	2.7978 (3)	484.73 (5)
			32.77 (16)*	9.3870 (1)	9.204 (1)	2.7949 (3)	482.90 (5)
			34.48 (12)*	9.3689 (1)	9.177 (1)	2.7906 (3)	479.80 (5)
			35.38 (13)*	9.3622 (1)	9.170 (1)	2.7896 (3)	478.93 (5)
			36.15 (14)*	9.3513 (1)	9.152 (1)	2.7846 (3)	476.57 (5)
			37.73 (16)*	9.3353 (1)	9.141 (1)	2.7806 (3)	474.48 (5)
			38.20 (27)*	9.3247 (1)	9.138 (1)	2.7795 (3)	473.66 (5)
			39.55 (23)*	9.3147 (1)	9.128 (1)	2.7729 (3)	471.48 (5)

Pressure values with * signals and corresponding lattice parameters are from DAC experiment. Number in parentheses represents the error of pressure or lattice parameter. The data for CM_{afm} $MnFe_2O_4$ at ambient conditions were obtained after completely decompression

Results and discussion

High-pressure phase transformation and the new structure

Angle dispersive X-ray diffraction patterns were collected as a function of pressures up to 39.55 GPa at 300 K. Typical X-ray diffraction patterns are presented in Fig. 1a. A new weak peak appears at $2\theta = 13.604°$ at 18.36 GPa and becomes stronger at 21.34 GPa, while the peaks of spinel-type $MnFe_2O_4$ become weak and disappear after 22.31 GPa, indicating a mixture of the spinel and the new phase between 18.36 and 22.31 GPa due to the kinetics. It is noted that the peak broadening is observed above 10 GPa in Fig. 1a. This would be due to the deviatoric stress above 10 GPa when silicone oil was used as pressure medium (Klotz et al. 2009) and peak overlapping in high-pressure phase. The spinel and high-pressure phase coexisting over a rather large pressure range may also be owing to the pressure medium employed (Errandonea et al. 2005) and the slow kinetics at room temperature. The induced deviatoric stress by pressure medium and the peak overlapping yields a relatively larger error at higher pressure. The energy dispersive X-ray diffraction patterns were collected as a function of pressure up to 24.63 GPa, with typical ones presented in Fig. 1b. The X-ray diffraction pattern collected at 9.71 GPa after annealing clearly showed a phase transformation. The new phase did not transform back to spinel structure during

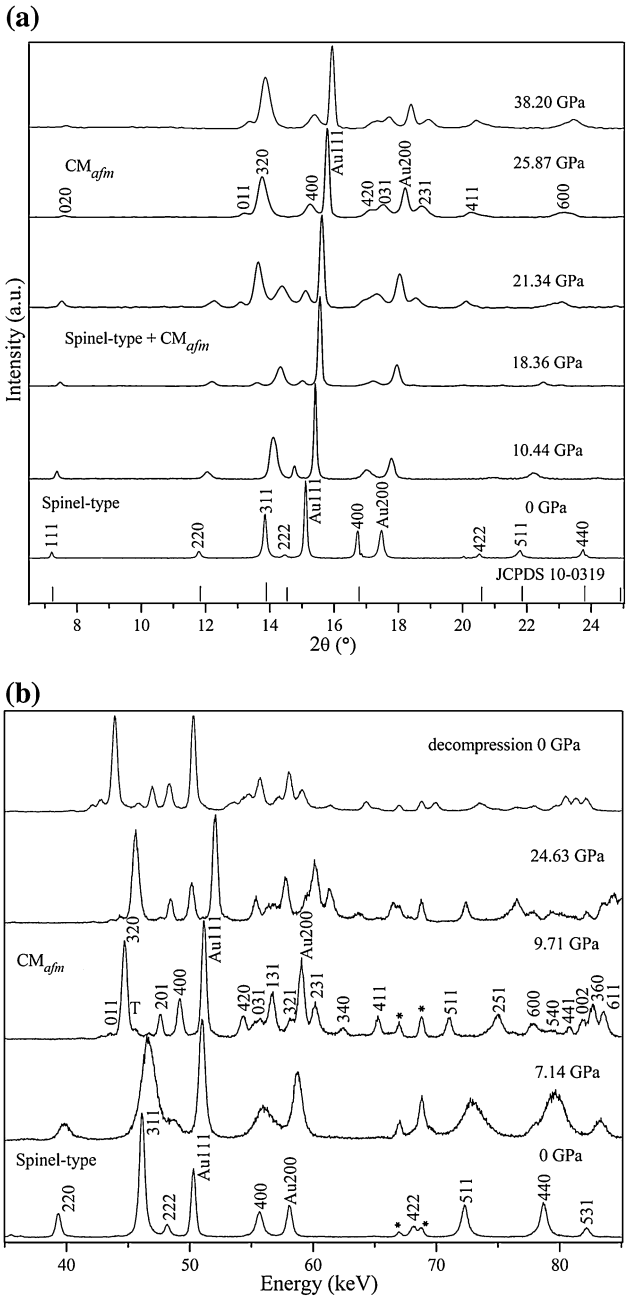

Fig. 1 Typical X-ray diffraction patterns of $MnFe_2O_4$ obtained by high-pressure ADXRD (**a**) and EDXRD (**b**) experiments. Abbreviations indexed to the diffraction peaks: Au = gold; * = X-ray fluorescence of Au

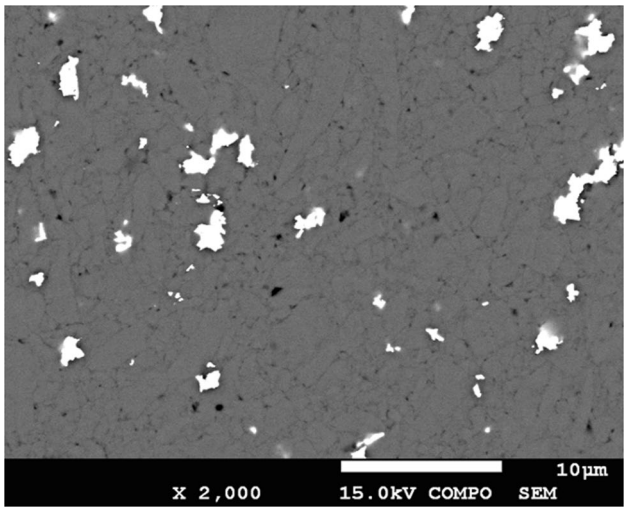

Fig. 2 Back-scattered electron image of recovered sample after annealing. The bright is Au and the gray is the high-pressure phase of $MnFe_2O_4$

decompression after annealing as illustrated in Fig. 1b. The recovered sample of the new phase was checked by scanning electron microscope. In Fig. 2, there are only two phases, including the pressure maker Au (bright) and another homogeneous phase with the chemical composition of $MnFe_2O_4$ (gray). Therefore, $MnFe_2O_4$ spinel transforms to a high-pressure polymorph. The transforming pressure is about 10 GPa at about 1000 K and about 18 GPa at room temperature. Though the phase boundary between the spinel-type and the high-pressure phase of $MnFe_2O_4$ possibly has a negative dP/dT slope, which is similar to that of $MgFe_2O_4$ reported by Levy et al. (2004), further study is required to precisely determine the phase boundary since the kinetics equilibrium is difficult to reach at room temperature.

For the structure of the high-pressure $MnFe_2O_4$ phase, there are some candidates including $CaFe_2O_4$-type, $CaTi_2O_4$-type, $CaMn_2O_4$-type and ε-$MgAl_2O_4$-type structures, as mentioned above. In order to refine the structure of the high-pressure phase, pure $MnFe_2O_4$ spinel was used as starting material and directly enclosed in TiB_2 heater to synthesize the high-pressure polymorph at about 12 GPa and 1473 K. An angle dispersive X-ray diffraction pattern of the quenched synthesized sample was additionally collected at ambient conditions at BL04B1 beamline, SPring-8, using monochromatic beam with energy of 51.00 keV. Because of the absence of the most intense lines, the ε-$MgAl_2O_4$-type structure was discarded. The Rietveld analysis was carried out based on $CaFe_2O_4$-type, $CaTi_2O_4$-type and $CaMn_2O_4$-type models, and the method was similar to that described by Andrault and Bolfan-Casanova (2001). The results indicate that $CaFe_2O_4$-type, $CaTi_2O_4$-type and $CaMn_2O_4$-type models are comparable in fitting the experimental data with wRp and Rp of 0.1431 and 0.1001, 0.1322 and 0.0876, and 0.1413 and 0.0965, respectively. The Rietveld fitting results for the three structures are shown in Fig. 3. Based on the fitting results, it is quite difficult to determine the structure for the high-pressure $MnFe_2O_4$ polymorph. Therefore, other method is required to search the most suitable structure for the high-pressure

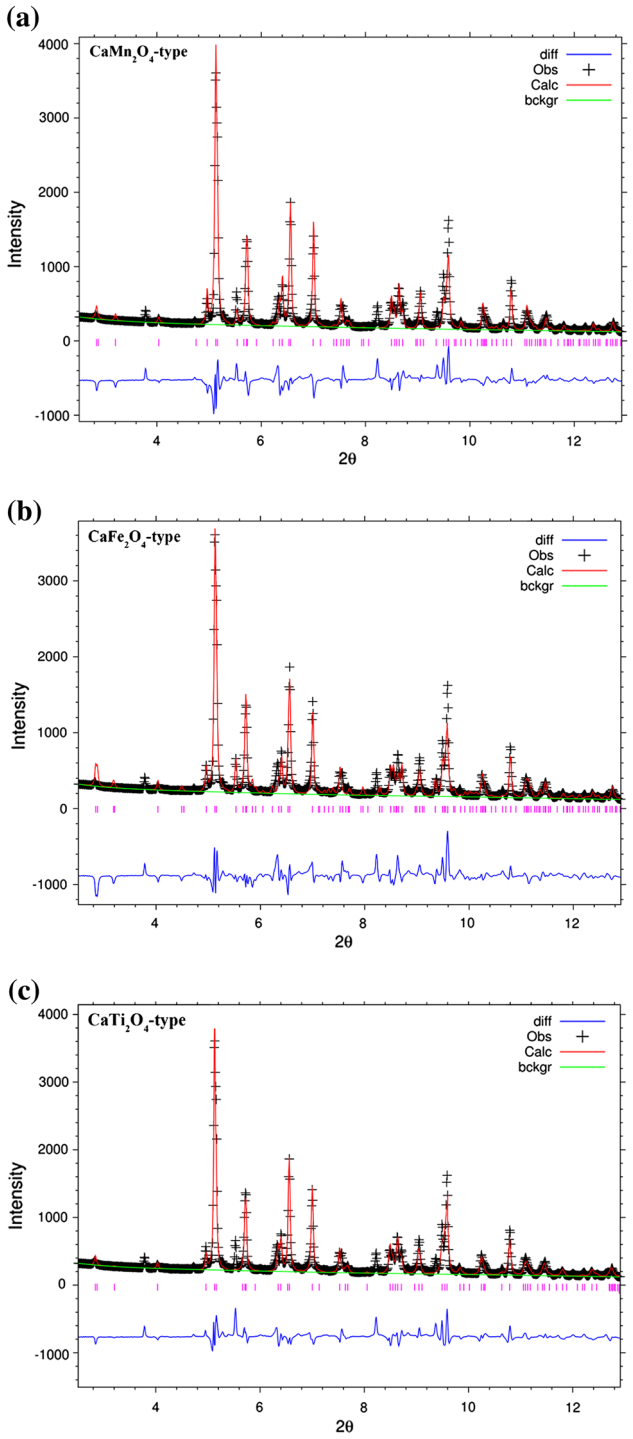

Fig. 3 Rietveld refinements of high-pressure $MnFe_2O_4$ polymorph's XRD pattern collected at ambient conditions. The *vertical bars* represent the high-pressure $MnFe_2O_4$ phase, and the *lower curve* represents the difference between observed and calculated profiles

$MnFe_2O_4$ phase, such as theoretical simulations proved to be effective for determining the structural stability. Considering the magnetic ordering, we designed six candidates,

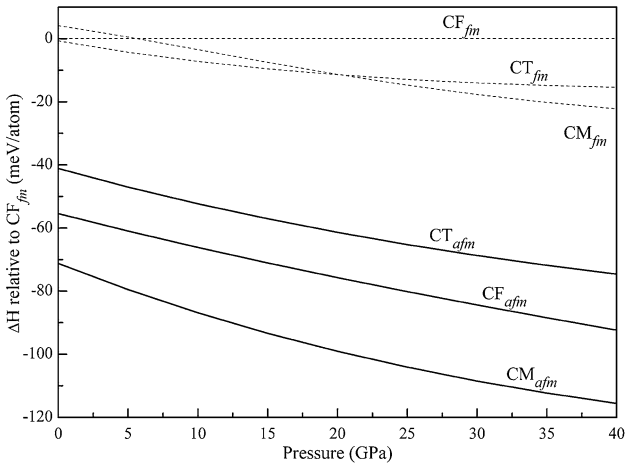

Fig. 4 Calculated relative enthalpy for ferromagnetic $CaFe_2O_4$-(CF_{fm}), $CaTi_2O_4$- (CT_{fm}) and $CaMn_2O_4$-type (CM_{fm}), and antiferromagnetic $CaFe_2O_4$- (CF_{afm}), $CaTi_2O_4$- (CT_{afm}) and $CaMn_2O_4$-type (CM_{afm}) $MnFe_2O_4$ as function of pressure

ferromagnetic $CaFe_2O_4$-type, $CaTi_2O_4$-type, $CaMn_2O_4$-type and antiferromagnetic $CaFe_2O_4$-type, $CaTi_2O_4$-type, $CaMn_2O_4$-type (labeled CF_{fm}, CT_{fm}, CM_{fm}, CF_{afm}, CT_{afm}, CM_{afm}, respectively). The GGA+U method implemented in the VASP code (Kresse and Furthmüller 1996; Kresse and Joubert 1999) is employed to deal with the strong correlation effect of the Mn and Fe electrons in our sample. Based on a previous investigation on spinel $MnFe_2O_4$ (Huang and Cheng 2013), the values of U for the on-site Coulomb interaction in the localized d orbitals and J for the screened exchange energy are set as 4 and 0.70 eV for Mn, and 4.5 and 0.89 eV for Fe, respectively. All the self-consistent calculations are converged until the total energy difference between electronic iterations being smaller than 10^{-7} eV per orthorhombic cell. The energy cutoff that determines the number of plane waves is 500 eV. The calculated different enthalpies compared to that of CF_{fm} are shown in Fig. 4. Obviously, CM_{afm} with the lowest enthalpy up to 40 GPa is proposed to be the most stable phase among those candidates. Thus, high-pressure $MnFe_2O_4$ polymorph in this work is assigned to be CM_{afm}, the antiferromagnetic $CaMn_2O_4$-type structure. The atomic positional parameters for the CM_{afm} $MnFe_2O_4$ were summarized in Table 2, and a structure model is illustrated in Fig. 5. The lattice parameters and volumes of CM_{afm} $MnFe_2O_4$ at different pressures are refined, as listed in Table 1. The phase transition leads the coordination of Mn^{2+} from fourfold to eightfold, while Fe^{3+} remains, yielding a denser polymorph.

P–V equation of state

The third-order Birch–Murnagham (BM3) (Birch 1947) equation of state (EoS) was used to fit the high-pressure

Table 2 Refined unit cell and atomic positional parameters for the CM_{afm} $MnFe_2O_4$ at ambient conditions

Space group: Pmab; Z = 4
a = 9.8680 (1) Å, b = 9.751 (1)Å, c = 2.9435 (2) Å

Atom	Wyck	x	y	z	
Mn	4d	0.75	0.1383 (10)	0.791 (5)	
Fe	8e	0.0757 (6)	0.1167 (8)	0.267 (4)	
O1	4c	0.00	0.25	0.686 (18)	
O2	4d	0.25	0.205 (4)	0.169 (13)	
O3	8e	0.117 (3)	−0.017 (4)	0.72 (4)	
Mn-O2	2.38 (4)	[1]	Fe-O1	2.28 (4)	[1]
Mn-O2	1.89 (4)	[1]	Fe-O1	1.940 (35)	[1]
Mn-O3	2.32 (8)	[2]	Fe-O2	1.946 (18)	[1]
Mn-O3	2.28 (7)	[2]	Fe-O3	2.12 (9)	[1]
			Fe-O3	1.91 (8)	[1]
			Fe-O3	2.135 (35)	[1]

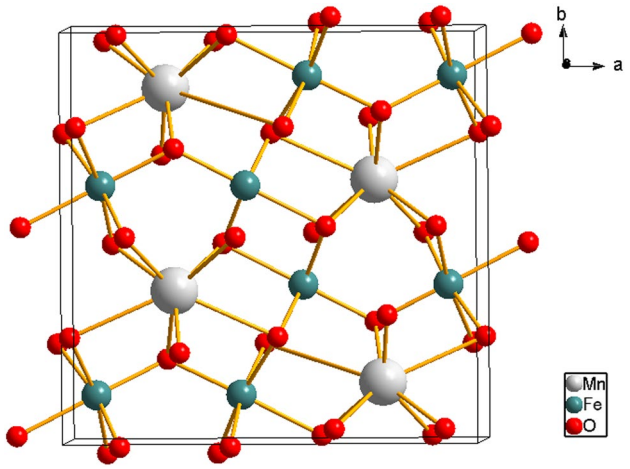

Fig. 5 Schematic view of the high-pressure CM_{afm} $MnFe_2O_4$

P–V data, yielding the bulk modulus of cubic spinel- and orthorhombic CM_{afm} $MnFe_2O_4$. The BM3 EoS can be expressed as follows:

$$P = \frac{3K_0}{2}\left[\left(\frac{V_0}{V}\right)^{\frac{7}{3}} - \left(\frac{V_0}{V}\right)^{\frac{5}{3}}\right]\left\{1 + \frac{3}{4}\left(K_0' - 4\right)\left[\left(\frac{V_0}{V}\right)^{\frac{2}{3}} - 1\right]\right\}$$

where K_0, K_0', and V_0 are the isothermal bulk modulus, its pressure derivation and the unit cell volume under ambient conditions, respectively. It is clear that silicone oil was used as pressure medium in the DAC experiment, and the non-hydrostatic effect is inevitable at higher pressures (Shen et al. 2004; Klotz et al. 2009). However, the X-ray diffraction peaks of sample and pressure marker Au were simultaneously collected in a very small spot. Therefore, non-hydrostatic effect is quite small, and all data from the DAC experiment can be used for fitting. The results from a least-squares fitting using an EosFit program (Angel 2001) are V_0 = 617.1 (2) Å^3, K_0 = 169.7 (35) GPa, and K_0' = 2.87 (40) for spinel-type $MnFe_2O_4$, and V_0 = 566.6 (2) Å^3, K_0 = 149.2 (24) GPa, and K_0' = 3.98 (19) for CM_{afm} $MnFe_2O_4$. The observed and refined unit cell volumes of spinel-type $MnFe_2O_4$ under ambient conditions are consistent with previous study (Passerine 1930). The unit cell volume data as a function of pressure and the compression curves calculated from the fitted parameters are plotted in Fig. 6. When the value of K_0' was set as 4, the isothermal bulk modulus K_0 was obtained as 160.6 (11) and 148.9 (7) GPa for spinel-type and CM_{afm} $MnFe_2O_4$, respectively. In previous study, the adiabatic bulk modulus (K_{S0}) for spinel-type $MnFe_2O_4$ was deduced as 161 GPa based on ultrasonic methods (Sakurai 1964). The orthorhombic CM_{afm} polymorph has a smaller isothermal bulk modulus compared with that of cubic spinel-type $MnFe_2O_4$. Due to the limitation of experimental technique, the degree of inversion has not been considered in this experiment. It may have little effect on the results since it could be covered by disturbances and uncertainties during measurement at high-pressure conditions (O'Neill and Dollase 1994).

In order to evaluate the quality of the Birch–Murnaghan EoS fitting, the relationships between the Eulerian strain (f_E) and the normalized pressure ($F = P/[3f_E(2f_E + 1)^{5/2}]$) for both phases were plotted in Fig. 7, where f_E is defined as $[(V_0/V)^{2/3} - 1]/2$. The f_E-F plot provides a visual indication to whether higher-order terms, such as K_0' and K_0'' (the isothermal bulk modulus' second-order pressure derivation

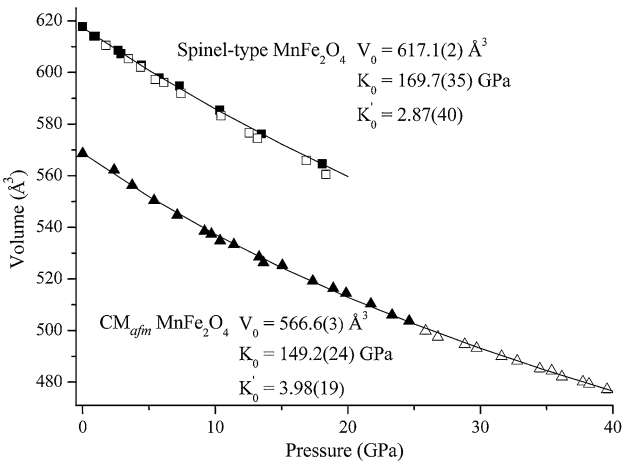

Fig. 6 Equation of state of the spinel-type and CM_{afm} $MnFe_2O_4$. *Solid* and *open symbols* are from multi-anvil and diamond anvil experiments, respectively. *Solid curve* represents the third-order Birch–Murnaghan equation fit for spinel-type phase with K_0 = 169.7 GPa and K_0' = 2.87, and *dashed curve* represents the third-order Birch–Murnaghan equation fit for CM_{afm} phase with K_0 = 149.2 GPa and K_0' = 3.98. The uncertainties of pressure and volume are within symbols

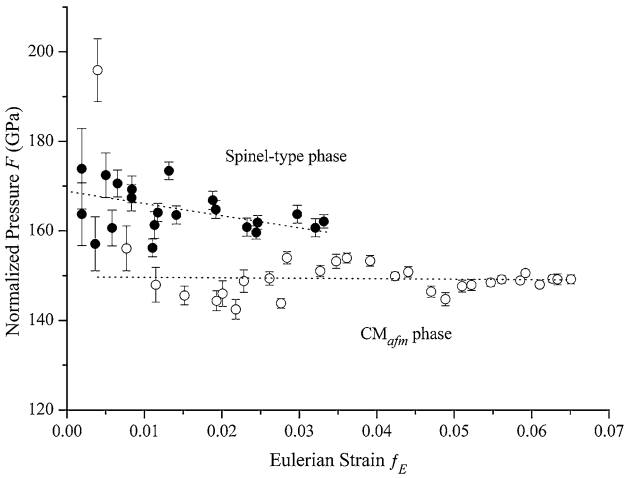

Fig. 7 Eulerian strain–normalized pressure (f_E-F) plots of spinel-type and CM$_{afm}$ polymorphs of $MnFe_2O_4$. *Solid* and *open circles* represent the data of spinel-type and CM$_{afm}$ phase, respectively. *Dotted lines* represent the linear fittings for both phases, respectively

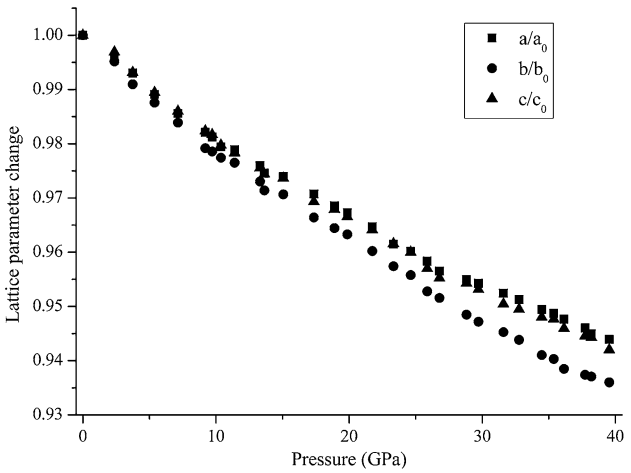

Fig. 8 Variations of a/a_0, b/b_0, and c/c_0 for CM$_{afm}$ $MnFe_2O_4$ as a function of pressure

at ambient conditions), are significant in the equation of state. The negative slope of the f_E-F plot indicates that the first pressure derivative of the bulk modulus is lower than 4. Therefore, the values of the derived K_0', 2.87 and 3.98 for spinel-type and CM$_{afm}$ $MnFe_2O_4$, are consistent with the f_E-F plot analysis. The near horizontal slope of CM$_{afm}$ phase is shallower than that of spinel-type phase, implying the derived K_0' of high-pressure phase is larger than that of spinel phase. It is consistent with the fitted results.

The unit cell parameters of CM$_{afm}$ $MnFe_2O_4$ as functions of pressure are plotted in Fig. 8. The divergence of the unit cell parameters indicates an anisotropic elasticity of CM$_{afm}$ $MnFe_2O_4$. By fitting a "linearized" third-order Birch–Murnaghan EoS, simply by substituting the cube of the lattice parameter for the volume (Litasov et al. 2007; Zhai et al. 2011) and following the procedure implemented in the EosFit program (Angel 2001), we can obtain the axial compressible modulus parameters. For comparison, the K_0' was fixed as 4. The analysis yields the axial compressibilities for *a*-, *b*- and *c*-axis are $K_a = 159.9$ (16) GPa, $K_b = 133.3$ (12) GPa and $K_c = 155.8$ (21) GPa, respectively, indicating the anisotropic elasticity along the axes.

The effect of A^{2+} cation substitution on the isothermal bulk modulus of Fe^{3+}-bearing spinel and on the phase transition pressure can be evaluated by comparing the present results with previous studies, as summarized in Table 3. It is noted that different studies may yield various results for the same compound. The radii of Mg^{2+}, Co^{2+}, Zn^{2+}, Fe^{2+} and Mn^{2+} with four coordination are 0.57, 0.58, 0.60, 0.63 and 0.66 Å (Shannon 1976), respectively. Based on the original data reported in references, the isothermal bulk modulus of different spinel was recalculated by fixing K_0' as 4, as listed in Table 3. Generally, the isothermal bulk modulus K_0 of Fe^{3+}-bearing spinel decreases with the increasing of radius of divalent cation, except that of Fe_3O_4. However, for the high-pressure polymorphs, CM$_{afm}$ $MnFe_2O_4$ shows a slight larger isothermal bulk modulus than those of $CaMn_2O_4$-type $MgFe_2O_4$ and $CaFe_2O_4$-type $CoFe_2O_4$, indicating that the isothermal bulk modulus of Fe^{3+}-bearing post-spinel phase increases with the increasing of radius of divalent cation.

In previous studies, some Fe^{3+}-bearing spinels were reported to transform into orthorhombic high-pressure phases at ambient temperature or after annealing, as summarized in Table 3. The phase transition pressures of $MgFe_2O_4$, $CoFe_2O_4$, $ZnFe_2O_4$, and $MnFe_2O_4$ at ambient temperature are 30, 27, 24.5 and 18 GPa, respectively. After annealing, the phase transition of $MgFe_2O_4$, Fe_3O_4 and $MnFe_2O_4$ was observed at pressure of 25, 23.6 and 9.7 GPa, respectively, indicating that the phase transition pressure of the same Fe^{3+}-bearing spinel decreases with heating. Therefore, it seems that the phase transition pressures of Fe^{3+}-bearing spinels decrease with the increasing of radii of divalent cations.

Conclusions

High-pressure in situ synchrotron X-ray diffraction experiments of $MnFe_2O_4$ were carried out up to 39.55 GPa at room temperature by using diamond anvil cell and multi-anvil apparatus. A phase transition was observed at about 18 GPa, and the high-pressure phase was determined as a CM$_{afm}$ structure. Fitting the *P*–*V* data to a third-order Birch–Murnaghan equation of state, the isothermal bulk modulus values and the first pressure derivatives were

Table 3 Comparison of isothermal bulk moduli and pressure (P_{Tr}) of transformation for Fe^{3+}-bearing oxide spinels and their high-pressure forms

Compound	Structure	K_0 (GPa)	K_0'	References	P_{Tr} (GPa)	References
$MgFe_2O_4$	Spinel-type	195	4 (fixed)	Andrault and Bolfan-Casanova (2001)	25[b]	Andrault and Bolfan-Casanova (2001)
	Spinel-type	209[a]	4 (fixed)	Levy et al. (2004)	27.7	Wang et al. (2002)
	$CaMn_2O_4$-type	142	4 (fixed)	Andrault and Bolfan-Casanova (2001)	30	Greenberg et al. (2009)
$CoFe_2O_4$	Spinel-type	178[a]	4 (fixed)	Greenberg et al. (2009)	27	Greenberg et al. (2009)
	$CaFe_2O_4$-type	145	4 (fixed)	Wang et al. (2003)		
$ZnFe_2O_4$	Spinel-type	176[a]	4 (fixed)	Greenberg et al. (2009)	24.5	Levy et al. 2000
$FeFe_2O_4$	Spinel-type	183	4 (fixed)	Mao et al. (1974)	23.6[b]	Fei et al. (1999)
	Spinel-type	181	5.5	Nakagiri et al. (1986)		
	Spinel-type	215	7.5	Gerward and Staun (1995)		
	Spinel-type	217	4 (fixed)	Haavik et al. (2000)		
	Spinel-type	186	5.1	Reichmann and Jacobsen (2004)		
$MnFe_2O_4$	Spinel-type	170	2.87	This study	18	This study
	Spinel-type	161	4 (fixed)	This study	9.7[b]	This study
	CM_{afm}	149	3.98	This study		
	CM_{afm}	149	4 (fixed)	This study		

[a] Recalculated isothermal bulk moduli using data from the references

[b] Result after annealing

obtained as $K_0 = 169.7$ (35) GPa, $K_0' = 2.87$ (40) for spinel-type $MnFe_2O_4$, and $K_0 = 149.2$ (24) GPa, $K_0' = 3.98$ (19) for CM_{afm} $MnFe_2O_4$, respectively. If K_0' is fixed to 4, K_0 was obtained as 160.6 (11) GPa for spinel-type $MnFe_2O_4$ and 148.9 (7) GPa for CM_{afm} $MnFe_2O_4$. Analysis of the axial compressibilities of orthorhombic CM_{afm} $MnFe_2O_4$ shows an anisotropic elastic behavior along the axes since the *b*-axis is more compressible than the *a*- and *c*-axis. Combined with previous results, the phase transition pressures of Fe^{3+}-bearing spinels decrease with the increasing of radii of divalent cations.

Acknowledgments The authors thank F. Qin, J. Niu, D. Yamazaki, N. Tsujino, M. Sakurai, F. Xu, W. Sun and E. Ito for their experimental helps. We thank Prof. T. Tsuchiya for his editorial handling and important suggestion. Critical comments and suggestion from two anonymous reviewers are helpful to improve the manuscript. The synchrotron radiation experiments were conducted at BL15U1, SSRF, China, and BL04B1, SPring-8, Japan (Proposal No. 2013B1257 and 2014A1736), respectively. This work was financially supported by National Natural Science Foundation of China (Grant No. 41372040), the Knowledge Innovation Program of the Institute of Geochemistry, Chinese Academy of Sciences, and the Visiting Researcher's Program of the Institute for Study of the Earth's Interior, Okayama University.

References

Andrault D, Bolfan-Casanova N (2001) High-pressure phase transformations in the $MgFe_2O_4$ and Fe_2O_3-$MgSiO_3$ system. Phys Chem Minerals 28:211–217

Angel RJ (2001) Equations of state. Rev Mineral Geochem 41: 35–60

Birch F (1947) Finite elastic strain of cubic crystals. Phys Rev 71:809–924

Chen M, Shu JF, Mao HK (2008) Xieite, a new mineral of high-pressure $FeCr_2O_4$ polymorph. Chinese Sci Bull 53:3341–3345

Errandonea D (2014) AB_2O_4 compounds at high pressure. In: Manjón FJ (ed) Pressure-induced phase transitions in AB_2X_4 chalcogenide compounds. Springer, Berlin, pp 53–73

Errandonea D, Meng Y, Somayazulu M, Häusermann D (2005) Pressure-induced α → ω transition in titanium metal: a systematic study of the effects of uniaxial stress. Phys B 355:116–125

Errandonea D, Kumar RS, Manjon FJ, Ursaki VV, Rusu EV (2009) Post-spinel transformations and equation of state in $ZnGa_2O_4$: determination at high pressure by in situ X-ray diffraction. Phys Rev B 79:024103

Fei YW, Frost DJ, Mao HK, Prewitt CT, Hausermann D (1999) In situ structure determination of the high-pressure phase of Fe_3O_4. Am Mineral 84:203–206

Frost BR, Shive PN (1986) Magnetic mineralogy of the lower continental crust. J Geophys Res 91:6513–6521

Gerward L, Staun OJ (1995) High-pressure studies of magnetite and magnesioferrite using synchrotron radiation. Appl Radiat Isotopes 46:553–554

Greenberg E, Rozenberg GK, Xu W, Arielly R, Pasternak MP, Melchior A, Garbarino G, Dubrovinsky LS (2009) On the compressibility of ferrite spinels: a high-pressure X-ray diffraction study of MFe2O4 (M = Mg Co, Zn). High Press Res 29:764–779

Haavik C, Tolen S, Fjellvag H, Hanfland M, Hauserman D (2000) Equation of state of magnetite and its high-pressure modification: thermodynamics of Fe-O system at high pressure. Am Mineral 85:514–523

Hammersley AP, Svensson SO, Hanfland M, Fitch AN, Hüusermann D (1996) Two-dimensional detector software: from real detector to idealised image or two-theta scan. High Press Res 14:235–248

Hastings JM, Corliss LM (1956) Neutron diffraction study of manganese ferrite. Phys Rev 104:328–331

Huang JR, Cheng C (2013) Cation and magnetic orders in $MnFe_2O_4$ from density functional calculations. J Appl Phys 113:033912

Irifune T, Fujino K, Ohtani E (1991) A new high-pressure form of $MgAl_2O_4$. Nature 349:409–411

Irifune T, Naka H, Sanehira T, Inoue T, Funakoshi K (2002) In situ X-ray observations of phase transitions in $MgAl_2O_4$ spinel to 40 GPa using multianvil apparatus with sintered diamond anvils. Phys Chem Minerals 29:645–654

Klotz S, Chervin J, Munsch P, Le Marchand G (2009) Hydrostatic limits of 11 pressure transmitting media. J Phys D Appl Phys 42:075413

Kresse G, Furthmüller J (1996) Efficient iterative schemes for ab initio total-energy calculations using a plane-wave basis set. Phys Rev B 54:11169–11186

Kresse G, Joubert J (1999) From ultrasoft pseudopotentials to the projector augmented wave method. Phys Rev B 59:1758–1775

Larson AC, Von Dreele RB (2004) General structure analysis system (GSAS). Los Alamos National Laboratory Report LAUR, pp 86–748

Levy D, Pavese A, Hanfland M (2000) Phase transition of synthetic zinc ferrite spinel ($ZnFe_2O_4$) at high pressure, from synchrotron X-ray powder diffraction. Phys Chem Minerals 27:638–644

Levy D, Pavese A, Sani A, Pischedda V (2001) Structure and compressibility of synthetic $ZnAl_2O_4$ (gahnite) under high-pressure conditions, from synchrotron X-ray powder diffraction. Phys Chem Minerals 28:612–618

Levy D, Diella V, Dapiaggi M, Sani A, Gemmi M, Pavese A (2004) Equation of state, structural behaviour and phase diagram of synthetic $MgFe_2O_4$, as a function of pressure and temperature. Phys Chem Minerals 31:122–129

Litasov KD, Ohtani E, Suzuki A, Funakoshi K (2007) The compressibility of Fe- and Al-bearing phase D to 30 GPa. Phys Chem Minerals 34:159–167

Liu LG (1978) A new high-pressure phase of spinel. Earth Planet Sci Lett 41:398–404

Mao HK, Takahashi T, Bassett WA, Kinsland GL, Merrill L (1974) Isothermal compression of magnetite to 320 KB. J Geophys Res 79:1165–1170

Nakagiri N, Manghnani MH, Ming LC, Kimura S (1986) Crystal structure of magnetite under pressure. Phys Chem Minerals 13:238–244

O'Neill HSC, Dollase WA (1994) Crystal structures and cation distributions in simple spinels from powder XRD structural refinement: $MgCr_2O_4$, $ZnCr_2O_4$, Fe_3O_4 and the temperature dependence of the cation distribution in $ZnAl_2O_4$. Phys Chem Minerals 20:541–555

O'Neill HSC, Wall VJ (1987) The olivine-spinel oxygen geobarometer, the nickel precipitation curve and the oxygen fugacity of the upper mantle. J Petrol 28:1169–1192

Ono S, Kikegawa T, Ohishi Y (2006) The stability and compressibility of $MgAl_2O_4$ high pressure polymorphs. Phys Chem Minerals 33:200–206

Passerine L (1930) Ricerche sugli Spinelli: II. I Composti. $CuAl_2O_4$, $MgAl_2O_4$, $MgFe_2O_4$, $ZnAl_2O_4$, $ZnCr_2O_4$, $ZnFe_2O_4$, $MnFe_2O_4$. Gazz Chim Ital 60:389–399

Reichmann HJ, Jacobsen SD (2004) High-pressure elasticity of a natural magnetite crysta. Am Mineral 89:1061–1066

Roeder PL (1994) Chromite: from the fiery rain of chondrules to the Kilauea Iki lava lake. Can Mineral 32:729–746

Sakurai J (1964) Ultrasonic propagation in nickel and Mn-ferrite at high magnetic fields. J Phys Soc Jpn 19:311–317

Shannon RD (1976) Revised effective ionic radii and systematic studies of interatomic distances in halides and chalcogenides. Acta Crystallogr A 32:751–767

Shen Y, Kumar RS, Pravica M, Nicol MF (2004) Characteristics of silicone fluid as a pressure transmitting medium in diamond anvil cells. Rev Sci Instrum 75:4450–4454

Tsuchiya T (2003) First-principles prediction of the *P-V-T* equation of state of gold and the 660-km discontinuity in Earth's mantle. J Geophys Res 108:2462. doi:10.1029/2003JB002446

Wang A, Saxena SK, Zha CS (2002) In situ X-ray diffraction and Raman spectroscopy of pressure-induced phase transformation in spinel Zn_2TiO_4. Phys Rev B 66:024103

Wang Z, Downs RT, Pischedda V, Shetty R, Saxena SK, Zha CS, Zhao YS, Schiferl D, Waskowsha A (2003) High-pressure x-ray diffraction and Raman spectroscopic studies of the tetragonal spinel $CoFe_2O_4$. Phys Rev B 68:094101

Wu Y, Wu X, Qin S, Yang K (2013) Compressibility and phase transition of intermetallic compound Fe_2Ti. J Alloys Compd 558:160–163

Xu C, Zhai S, Ye L, Wu X, Yang K (2014) X-ray diffraction studies of $Sr_3Cr_2O_8$ and $Ba_3Cr_2O_8$ at high pressures. Solid State Commun 200:5–8

Yamanaka T, Uchida A, Nakamoto Y (2008) Structural transition of post-spinel phases $CaMn_2O_4$, $CaFe_2O_4$ and $CaTi_2O_4$ under high pressure up to 80 GPa. Am Mineral 93:1874–1881

Yong W, Botis S, Shieh SR, Shi W, Withers AC (2012) Pressure-induced phase transition study of magnesiochromite ($MgCr_2O_4$) by Raman spectroscopy and X-ray diffraction. Phys Earth Planet Inter 196:75–82

Zhai S, Xue W, Yamazaki D, Shan S, Ito E, Tomioka N, Shimojuku A, Funakoshi K (2011) Compressibility of strontium orthophosphate $Sr_3(PO_4)_2$ at high pressure. Phys Chem Minerals 38:357–361

Zhai S, Shan S, Yamazaki D, Funakoshi K (2013) Compressibility of pyrochlore-type $MgZrSi_2O_7$ determined by in situ X-ray diffraction in a large-volume high pressure apparatus. High Press Res 33:1–7